AGU PUBLICATIONS

Geochemistry, Geophysics, Geosystems

RESEARCH ARTICLE
10.1002/2017GC007091

Special Section:
Magnetism From Atomic to Planetary Scales: Physical Principles and Interdisciplinary Applications in Geo- and Planetary Sciences

Magnetic Properties and Paleomagnetism of Zebra Rock, Western Australia: Chemical Remanence Acquisition in Hematite Pigment and Ediacaran Geomagnetic Field Behavior

Alexandra Abrajevitch[1,2], Brad J. Pillans[3], Andrew P. Roberts[3], and Kazuto Kodama[4]

[1]Department of Earth Sciences, Ehime University, Matsuyama, Japan, [2]Institute of Tectonics and Geophysics, Russian Academy of Sciences, Khabarovsk, Russia, [3]Research School of Earth Sciences, Australian National University, Canberra, ACT, Australia, [4]Research Center for Knowledge Science in Cultural Heritage, Doshisha University, Kyoto, Japan

Abstract Zebra Rock, a decorative stone remarkable for its unusual pattern of regularly spaced reddish bands and rods with white background, is found within the Neoproterozoic succession in East Kimberley, Western Australia. The unusual pigment distribution suggests that precipitation of hematite, or its precursor phase, occurred in a single episode. Magnetic properties of hematite pigment in Zebra Rock are distinctly different from those of the host shale, with a smaller median particle size and higher degree of structural perfection. The low thermal stability of the Zebra Rock pigment, with onset of thermal alteration at 300°C, suggests that the rocks have not undergone significant metamorphic heating. Stepwise thermal demagnetization reveals multiple magnetization components. Short-range variability in the relative contributions of the components to the total remanence is indicative of the stochastic nature of the hematite pigment growth process. In addition to seven magnetization components with shallow to intermediate inclinations that can be matched to the Paleozoic Australian apparent polar wander path, Zebra Rock samples contain a distinct steeply dipping magnetization that is not observed in the host shales. The steep magnetization appears to be primary, based on its unique association with the Zebra pattern, dissimilarity with younger directions, and evidence for low degree of thermal alteration of the rocks. The steep characteristic remanence contrasts with previous paleomagnetic indications of low Australian Neoproterozoic paleolatitudes. The characteristic Zebra Rock magnetization is the first Australian example of incompatible magnetization directions that have been reported previously from Ediacaran rocks in Laurentia, Baltica, and Africa.

Key Points:
- Paleomagnetic study of Zebra Rock from East Kimberley, Western Australia reveals multiple magnetization components
- Short-range variability in the remanence components is indicative of the stochastic nature of the hematite pigment growth process
- The steep characteristic Zebra Rock magnetization is the first Australian example of incompatible Ediacaran magnetizations

Supporting Information:
- Supporting Information S1

Correspondence to:
A. Abrajevitch,
alexandra.abrajevitch@gmail.com

Citation:
Abrajevitch, A., Pillans, B. J., Roberts, A. P., & Kodama, K. (2018). Magnetic properties and paleomagnetism of Zebra Rock, Western Australia: Chemical remanence acquisition in hematite pigment and Ediacaran geomagnetic field behavior. *Geochemistry, Geophysics, Geosystems*, *19*, 732–748. https://doi.org/10.1002/2017GC007091

Received 27 JUN 2017
Accepted 20 FEB 2018
Accepted article online 26 FEB 2018
Published online 13 MAR 2018

1. Introduction

Hematite pigment is a common constituent of sedimentary rocks and can carry a highly stable remanent magnetization that is resistant to partial heating and chemical alteration under oxidizing conditions at Earth's surface (Dunlop & Özdemir, 1997). While multiple hematite formation episodes, often associated with fluid migration (e.g., Park, 1997; Ricordel et al., 2007), can reset or obscure primary magnetizations, precipitation of authigenic hematite is a nonuniform process that is controlled by interactions between matrix rocks and iron-bearing fluids (e.g., Jamtveit & Hammer, 2012). Some pockets within sedimentary formations are less affected by pigment formation due to local variations in solute transport pathways, such as porosity networks or fracture systems (e.g., Abrajevitch et al., 2014; Liu et al., 2011). Such unaltered pockets, if recognized, offer opportunities to recover an earlier paleomagnetic signal, and to understand basic remanence acquisition processes. Unusual hematite pigment distributions in Zebra Rock suggest that it may represent such a diagenetic refugium.

Zebra Rock is remarkable for its rhythmic patterns of reddish-brown bands, rods, and elliptical spots on a white or light-colored background (Figure 1). The rock is found in small discontinuous outcrops of stratified claystone (the Johnny Cake Shale Member) within the Late Proterozoic Ranford Formation (Dow & Gemuts, 1969). Known Zebra Rock occurrences are restricted to a relatively small area near Ord River in the East Kimberley region, Western Australia (Figure 1). Fine-grained indurated claystone of Zebra Rock is composed largely of quartz and sericite, with minor alunite, hematite, kaolinite, and its polymorph dickite (Loughnan & Roberts, 1990). The white and reddish-brown zones are similar in composition; their main difference is the greater concentration of ferric oxide in the latter (Loughnan & Roberts, 1990). Formation of the unique

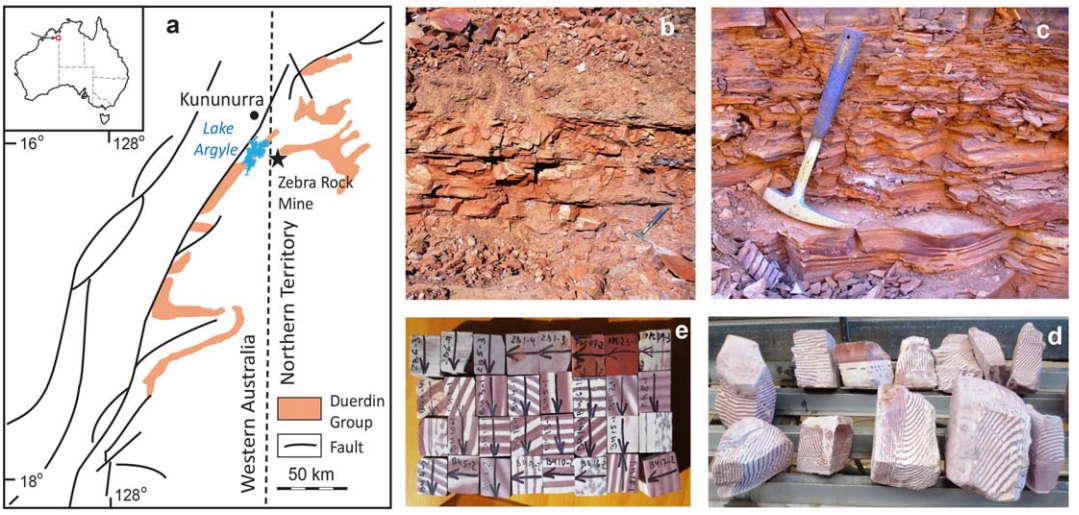

Figure 1. (a) Location of the Zebra Rock Mine near Kununurra, East Kimberley, Western Australia. Simplified geological sketch map with distribution of the late Neoproterozoic Duerdin Group, the youngest member of which, the Ranford Formation, hosts Zebra Rock. (b) Host shales of the Johnny Cake shale member of the Ranford Formation and (c) a bed of Zebra Rock exposed at the Zebra Rock Mine. Examples of the Zebra pattern in Figure 1d block samples and (e) paleomagnetic specimens. The Zebra patterning is not so clearly evident in field photographs in Figures 1b and 1c because the outcrop is covered by a fine red dust, but the highly variable patterns are evident in block samples (d) and paleomagnetic specimens.

Zebra Rock patterns has long puzzled geologists. In early studies, hematite segregation in distinct bands was explained by sedimentation processes, either by introduction at regular intervals of hydrated iron oxides during sedimentation in a marine environment (Larcombe, 1924, 1926) or by accumulation of ferruginous minerals in ripple troughs (Geidans, 1981), or, alternatively, by postdepositional alteration, either through acidic leaching around probable pyrite crystals (*Clarke* in Hobson, 1930), or through iron oxide mobilization-reprecipitation that accompanied groundwater circulation along bedding and joint planes (Hancock, 1968).

Reexamination of Zebra Rock mineral compositions by Loughnan and Roberts (1990) revealed unusual mineralogical relationships. While the quartz content is relatively uniform, kaolinite and dickite, two polytypes of the kaolin group, and the K-bearing and Al-bearing minerals sericite and alunite, tend to have an inverse abundance with respect to each other. The presence of dickite, formation of which is restricted to hydrothermal or authigenic processes (e.g., Ross & Kerr, 1930), and alunite, which typically forms as an alteration product of K-rich materials in sulfate-rich weakly acidic solutions (e.g., Dill, 2001), testifies to a diagenetic origin of Zebra Rock. Based on the unusual mineralogical associations, Loughnan and Roberts (1990) suggested that fluctuating pH of interstitial solutions during or immediately following deposition of an initial fine-grained sediment created an environment conducive to ferrous ion oxidation with formation of dispersed colloidal Fe_2O_3 particles. With increasing concentration, periodic coagulation was inferred to have led to development of well-defined diffusion or Liesegang banding. However, Mattievich et al. (2002, 2003) noted that neither sedimentary processes, nor postdepositional leaching, nor periodic (Liesegang-type) precipitation can explain the Zebra patterns, where bands evolve into rods or ellipses, with occasional forking into two bands, and the frequently observed large angles between sedimentary bedding and the red and white pattern. Observation of a common preferred orientation of kaolinite and hematite particles in Zebra Rock led Mattievich et al. (2002, 2003) to suggest that the diverse banding features can be explained as a relict of a liquid crystal phase. In their model, a liquid-crystalline aqueous clay suspension was infiltrated by a ferrous solution to form a nematic phase (where particles orient in loose parallel lines). A ferronematic was formed as ferrihydrite, a likely initial precipitate, transformed to hematite, which shares a common growth habit with kaolinite. With increased hematite particle size (and magnetic moment per particle), magnetic dipole-dipole interactions caused particles to aggregate by sliding sideways between kaolinite platelets, creating the red and white banding. The variety of banding patterns was argued to have been created by competition between edge effects determined by sedimentary bedding and the geomagnetic torque

exerted on hematite particles. Mattievich et al. (2003) estimated that hematite particles with sizes of tens of nanometers have sufficient magnetic moment to drive changes in preferred particle orientation in Earth-like magnetic fields. A similar geomagnetic field influence on ferrihydrite aggregation has been documented to influence hematite and goethite growth (Jiang et al., 2016).

Regardless of its formation mode, either from periodic precipitation (Liesegang banding) or in liquid crystal mode, the hematite in Zebra Rock has formed chemically, likely from a ferrihydrite precursor. A narrow window of opportunity for developing appropriate conditions suggests that segregation of hematite pigment (or its precursor) occurred in a single episode. A single chemical seeding with succeeding hematite maturation provides an opportunity to evaluate remanence acquisition processes associated with pigment formation in Zebra Rock. Likewise, the paleomagnetic record of Zebra Rock is of interest for understanding Ediacaran geomagnetic field behavior.

2. Sampling and Methods

Samples for this study were collected from the Zebra Rock Mine, which is located about 70 km from Kununurra, just across the Western Australia border from the Northern Territory (Figure 1a). Here shale interbedded with siltstone of the Johnny Cake Shale Member of the Ranford Formation (Dow & Gemuts, 1969; Thorne et al., 1999) is exposed in an open pit mine (Figure 1b). Zebra Rock crops out in relatively thin, near-horizontal beds (Figure 1c). Oriented block samples of beds with the distinctive Zebra pattern (Figures 1c–1e) and samples from the host shales (Figure 1b) were collected for this study. A magnetic compass with inclinometer was used for sample orientation.

Block samples were cut into standard cubes in the laboratory with ~20 mm sides, which yielded 1–6 specimens per sample. Magnetic measurements were made at the Australian National University Black Mountain paleomagnetic laboratory and at the Center for Advanced Core Research, Kochi University, Japan. The natural remanent magnetization (NRM) of the specimens was measured with a 2-G Enterprises superconducting rock magnetometer. The specimens were progressively thermally demagnetized in air. Temperatures were progressively increased in steps ranging initially from 50°C at lower temperatures to 5°C at higher temperatures until <5% of the initial NRM intensity remained, up to a maximum temperature of 700°C. Effects of heating were monitored by measuring the low-field magnetic susceptibility after each heating step. All experiments were undertaken in magnetically shielded laboratories with residual fields <300 nT. Demagnetization data were plotted on orthogonal demagnetization diagrams (Zijderveld, 1967) and stereographic projections. Remanence directions were determined by principal component analysis (Kirschvink, 1980) on linear demagnetization trajectories using the Remasoft 3.0 software package (Chadima & Hrouda, 2006).

Magnetic characteristics of representative samples were also evaluated with rock magnetic measurements. Thermomagnetic curves were acquired with a multifunction Kappabridge system (AGICO Ltd., Brno) equipped with a furnace, with progressive heating in air to 700°C at 10°C/min, followed by cooling back to room temperature at the same rate. Values of saturation magnetization (M_s), saturation remanence (M_{rs}), and coercive force (B_c) were determined from hysteresis loops, which were measured from +1.5 to −1.5 T with a Princeton Measurements Corporation vibrating sample magnetometer (VSM). For several representative samples from the red Zebra pigment, hysteresis loops were also measured from +7 to −7 T with a Quantum Design Magnetic Property Measurement System (MPMS). The coercivity of remanence (B_{cr}) was obtained by demagnetizing M_{rs} in a stepwise increasing backfield. Low-temperature properties of representative samples were investigated with a MPMS. An IRM was imparted at 300 K in a 5 T field and was then measured at 5 K intervals, in zero-field, during cooling from 300 to 10 K, followed by warming from 10 to 400 K and then by cooling back to 300 K. Direct current (DC) susceptibility measurements were performed in a 5 mT applied field.

3. Results

3.1. Rock Magnetism

3.1.1. Thermomagnetic Runs

Monitoring of sample magnetization as a function of temperature provides important information about mineral-specific Curie or Néel temperatures (T_C and T_N), and about thermally induced chemical and

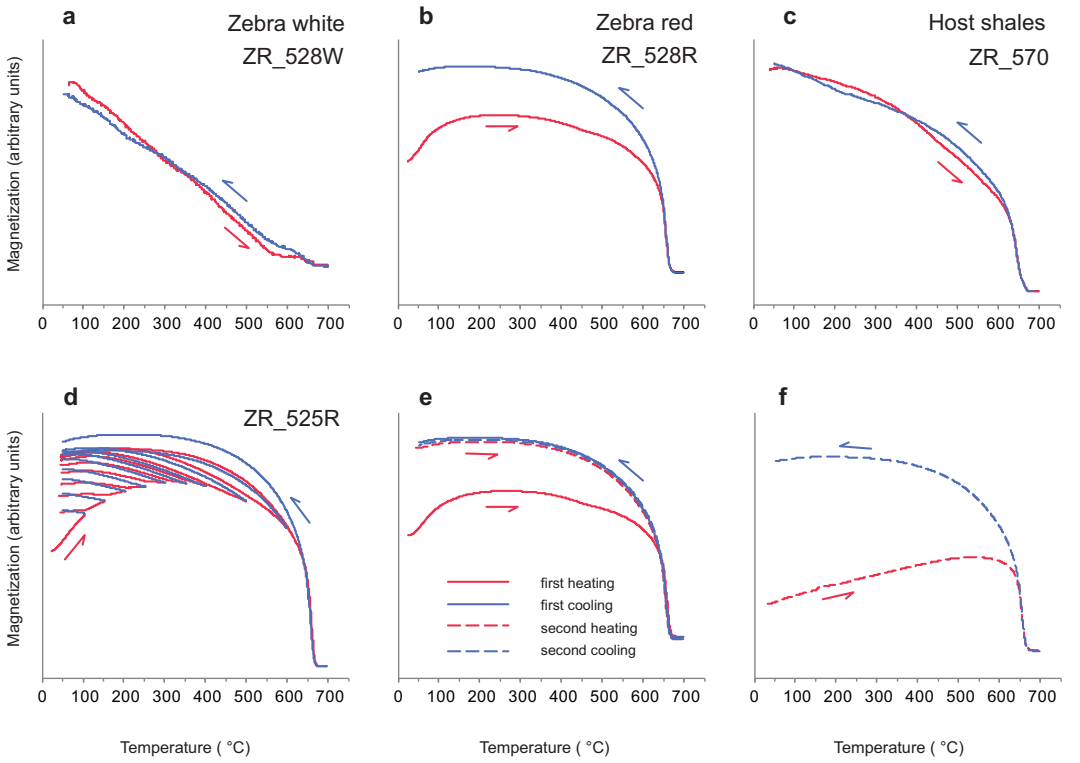

Figure 2. Thermomagnetic behavior of representative Zebra Rock samples. Red and blue lines denote heating and cooling curves, respectively. Behavior typical of (a) white stripes, (b) red stripes, and (c) host shales. Stepwise heating of (d) a red stripe sample indicates irreversible heating and cooling curves even at low peak temperatures. Differences in repeated heating curves obtained (e) without and (f) with stirring the sample between runs indicates that the irreversibility is partially due to magnetic moment alignment in an applied magnetic field.

structural changes in ferrimagnetic and canted antiferromagnetic minerals, respectively. Representative thermomagnetic runs for Zebra Rock samples are shown in Figure 2. The magnetization of host shale samples decreases progressively during heating (Figure 2c). A small change in slope is observed at ~400°C; the rate of decrease increases above 600°C on approach to the T_N of hematite. Cooling curves for host shale samples are similar to warming curves, albeit without the inflection at 400°C. Samples from white stripes in Zebra Rock undergo an almost linear magnetization decrease during heating to 550°C (Figure 2a). Small stepwise magnetization changes at 570 and 670°C are typical of the T_C and T_N of magnetite and hematite, respectively. Cooling curves are close to the warming curves, with a minor total decrease in magnetization at room temperature after the heating/cooling cycle.

Samples from red stripes in Zebra Rock undergo an initial magnetization increase during heating to 100°C (Figure 2b). On further heating, the magnetization plateaus at 200–350°C, and then decreases slowly to ~650°C, from where it decreases sharply up to T_N (Figure 2b). Estimated T_N values of red stripe samples range from 663 to 673°C. The cooling curve lies above the heating curves, and has a "blocky" shape that is typical of saturated hematite (e.g., Dunlop & Özdemir, 1997). Stepwise heating-cooling experiments for the red Zebra stripes (Figure 2d) demonstrate that irreversible magnetization increases occur at even the lowest heating temperatures. A second thermomagnetic run on a previously heated sample (without sample redispersion) is reversible and identical to the cooling curve from the initial run (Figure 2e).

The difference between thermomagnetic warming and cooling curves may indicate either irreversible chemical or structural changes, or may result from increased alignment of nonsaturated magnetic minerals on heating in an applied magnetic field. De Boer and Dekkers (1998) suggested that the two processes can be distinguished by stirring samples between consecutive thermomagnetic runs. In defect-poor hematite, the second run after sample redispersion is expected to be identical to the initial cycle. In our samples, the magnetization of the sample that was heated after repeated stirring (Figure 2f) is weaker than for the

sample that was heated repeatedly without stirring (Figure 2e), which suggests that the increased magnetization on heating is, at least in part, due to increased magnetic moment alignment in an applied field. However, the heating curve after stirring is not identical to the initial run. Magnetization values at room temperature at the beginning of the cycle are lower during the repeated run, and the warming curve has a longer interval of increasing magnetization values that reach a plateau at a higher temperature of ~500°C. Such a deviation from the initial run characteristics indicates that structural changes (annealing) occurred during heating. Small inflections at ~450°C, which are visible in initial warming curves but are absent in cooling curves and repeated heating runs (e.g., Figures 2b and 2e), may represent the annealing temperature, or the small addition of another magnetic phase that underwent mineralogical change at this temperature. Overall, thermomagnetic behavior indicates that hematite pigment in red stripes from Zebra Rock is stable at low heating temperatures and that it contains structural defects.

3.1.2. Hysteresis Measurements

Typical hysteresis loops for Zebra Rock varieties are shown in Figure 3. Hysteresis loops for white samples are noisy due to their low magnetization intensities; nevertheless, consistent patterns are evident (Figure 3a). Some samples have a negative magnetization at high positive applied fields that is typical of diamagnetic matrix minerals, while others have a positive magnetization that is typical of paramagnetic minerals. The different field dependence may be due to variable ferrimagnetic mineral concentrations in the white zones, or to variable matrix composition, e.g., ratio of diamagnetic quartz to paramagnetic clays, or, a combination of these factors. The loops are not closed at 1.5 T, which indicates the presence of a high coercivity mineral (hematite), and are distinctly wasp-waisted. The constriction can be indicative of mixtures of high and low coercivity minerals, or mixtures of magnetic particles with contrasting domain state (e.g., Roberts et al., 1995; Tauxe et al., 1996). Samples from the red stripes have wide hysteresis loops (Figure 3b) and are not saturated at the highest applied field of 1.7 T. Coercivity estimates from raw hysteresis loops (without high-field slope correction, which are, thus, underestimates) range between 480 and 520 mT. B_{cr} is determined from the axis-crossing point of the backfield remanence curves, and varies from 700 to 800 mT. To estimate saturation hysteresis values of the red stripe pigment, a hysteresis loop was measured to 7 T for a representative sample (Z539 red stripe) before (Figures 3d and 3f) and after heating to 700°C (Figures 3e and 3g). After correction for the high-field slope (estimated from the upper loop at high fields), the unheated sample has $B_c = 630$ mT, which increases to 1.75 T for the heated sample (Figures 3f and 3g). The coercivity of red host shales (Figure 3c) is lower than that of the red Zebra stripes, with B_c in the 280–370 mT range (uncorrected for high-field slope), and $B_{cr} = 530$–540 mT. Hysteresis loops for red matrix shales have a small, but distinct, wasp-waistedness.

3.1.3. Low-Temperature Remanence

Low-temperature magnetic measurements are used to identify magnetic phases based on characteristic temperature-dependent behavior of iron oxides. On cooling across the Verwey transition below ~120 K, magnetite converts from a high-temperature cubic phase to a low-temperature monoclinic phase, with an accompanying magnetization change. Hematite, a canted antiferromagnet with a small magnetic moment at room temperature, undergoes a magnetic phase transition (the Morin Transition) to a purely antiferromagnetic phase on cooling below 260 K (Morin, 1950; Schroeer & Nininger, 1967). Morin transition characteristics, such as its temperature (T_M, estimated from the inflection point of $M(T)$ curves), its width (ΔT_M, estimated from the full width at half maximum of dM/dT curves), the defect magnetization remaining below the transition, the difference in T_M values from cooling and warming cycles (thermal hysteresis), and the magnetic memory ratio (the fraction of initial remanence left after low-temperature cycling) are sensitive to grain-size and crystal imperfection density (Özdemir & Dunlop, 2006; Özdemir et al., 2008). In pure samples, the transition shifts to lower temperatures with decreasing hematite grain-size until it disappears below 30 nm (Özdemir et al., 2008). For the same cooling/warming rate, thermal hysteresis tends to be much greater in submicron hematite than in natural multidomain (MD) crystals (Özdemir et al., 2008). A larger ΔT_M may result from broad particle size distributions (Özdemir et al., 2008) Regardless of grain-size, higher SIRM memory ratios occur with higher defect moments below T_M (Özdemir & Dunlop, 2006).

Low-temperature cycling curves for representative samples are shown in Figure 4. An IRM was imparted in a 5 T field at room temperature, and was then cooled to 10 K and warmed back to 300 K in zero-field. White stripe samples (Figure 4a) have gradually increasing SIRM values on cooling, with an inflection at ~110 K, which likely corresponds to the Verwey transition in magnetite. On subsequent warming, SIRM decreases continuously, without inflections, and no identifiable Morin transition is observed. In heated samples (Figure 4b), magnetization does not change significantly between 300 and 250 K; below this temperature SIRM

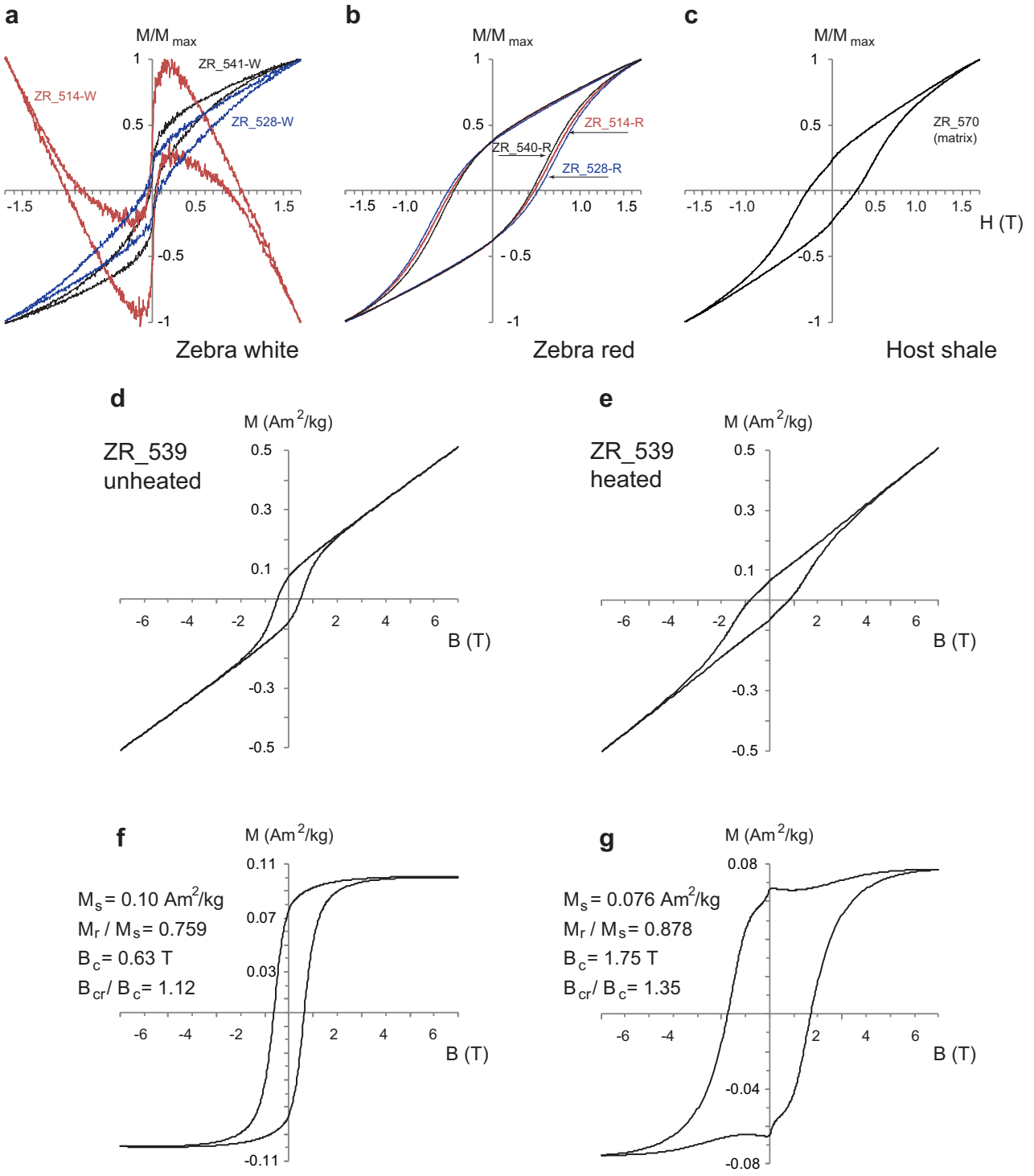

Figure 3. Representative hysteresis loops measured to a peak field of 1.5 T for representative examples of unheated (a) white and (b) red Zebra stripes, and (c) host shales. Hysteresis loops of a red Zebra stripe (sample ZR_539) measured to a peak field of 7 T (d and f) before and (e and g) after annealing at 700°C. Hysteresis loops (d and e) before and (f and g) after high-field slope correction.

decreases continuously. However, the total intensity loss on cooling to 10 K is small (~0.05% of the room temperature (RT) SIRM). Thus, in the unheated white stripe sample, hematite (as evident in hysteresis and IRM acquisition measurements) does not have a typical Morin transition signature, which indicates a small median size (below 30 nm) and/or high density of structural defects. The warming curve is separated from

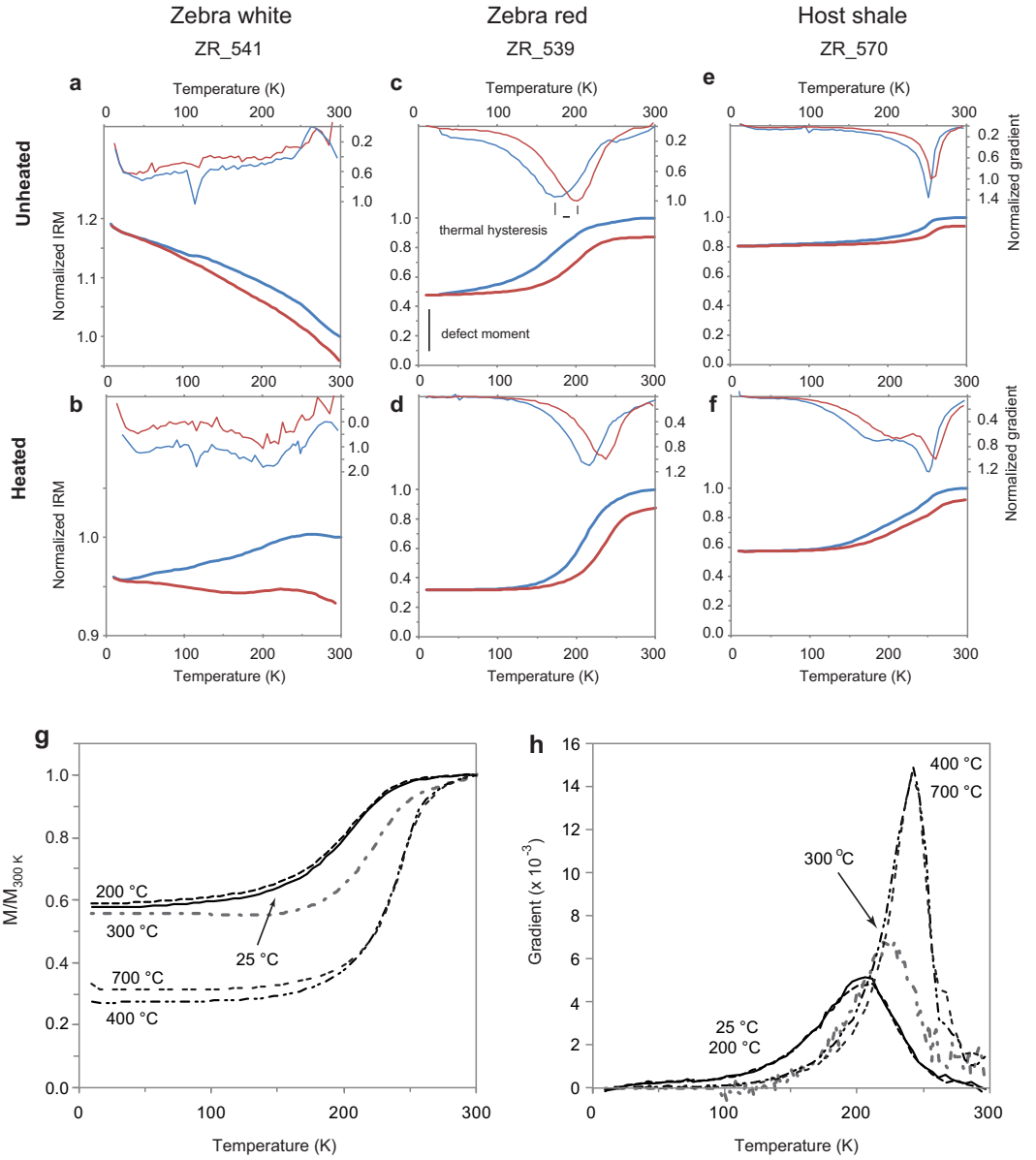

Figure 4. Low-temperature dependence of magnetization for representative samples of (a and b) white and (c and d) red Zebra stripes, and for (e and f) host shale (a, c, and e) before and (b, d, and f) after annealing at 700°C. Magnetization induced by a 5 mT DC field (measured on warming after cooling from 300 to 10 K in zero-field) in a red Zebra stripe sample after heating to the indicated peak temperatures as (g) linear and (h) gradient curves.

the cooling curve across the entire temperature range. Gradient curves, although noisy due to weak magnetization, have wide peaks with maxima at ~220 K, which indicates a suppressed Morin Transition. The transition observed in heated samples suggests that annealing increases the median size and/or structural integrity.

The SIRM of the red stripe samples (Figure 4c) is practically independent of temperature during cooling in the 300–240 K interval; it starts to decrease at the Morin Transition. The transition (T_M = ~178 K) is spread over a large temperature range. The main change occurs across 210–130 K, where ~60% of the initial RT SIRM is lost; the SIRM decrease then continues more slowly to 10 K. Warming curves for the unheated samples are separated from the cooling curves. SIRM is essentially flat from 10 to ~150 K, it rises in the 150–240 K range, and plateaus above 250 K. The defect moment of red Zebra pigment is ~48–52% of the RT SIRM; the thermal hysteresis is ~25 K and the magnetic memory ratio is 87–90%. In heated red Zebra

samples (Figure 4d), the transition is sharper, with a higher T_M of 214–222 K; ΔT_M decreases to 60 K, the defect moment decreases to 27–32%, while thermal hysteresis and magnetic memory ratios remain similar to those of unheated samples.

Unheated host shales (Figure 4e) have a distinct Morin transition. Compared to unheated red stripe samples, the transition in shale is much sharper ($\Delta T_M = 25$ K), it occurs at higher temperature ($T_M = 253$ K), it has smaller thermal hysteresis (6 K), a higher defect moment of ~80%, and a memory ratio of ~95%. In heated matrix samples (Figure 4f), the defect moment decreases to ~55% and the transition width increases significantly. Two peaks in the gradient curves suggest the presence of two hematite particle populations; one with a low T_M of ~180 K and ΔT_M of ~90 K, and large thermal hysteresis of ~35 K, and the second with a high T_M of ~251 K, a narrow ΔT_M (>30 K), and a small thermal hysteresis of ~9 K.

3.1.4. DC Susceptibility

Thermal stability of Zebra Rock hematite was evaluated by monitoring heating-induced changes in Morin transition parameters (Figures 4g and 4h). A magnetization induced in a red pigment sample (ZR-525R) by a 5 mT DC field was measured during warming after cooling from 300 to 10 K in zero-field. A fresh (unheated) sample was subjected to DC susceptibility measurements, and was then progressively heated to 200, 300, 400, and 700°C. After each heating step, the sample was cooled to RT, and DC susceptibility was measured. Morin transition characteristics of the sample heated to 200°C are similar to those of the fresh sample (Figures 4g and 4h). In the sample heated to 300°C, T_M increased to ~225 K, and the defect moment did not change greatly. Heating to 400°C increased the T_M to ~240 K and considerably decreased the defect moment. Further heating to 700°C did not produce significant changes. The onset of thermal alteration is, thus, estimated at ~300°C; heating to 400°C changes hematite pigment properties dramatically. Its low thermal stability suggests that Zebra Rock has not been heated above 300°C since the characteristic striped pattern formed.

3.2. Paleomagnetism

Examples of demagnetization behavior for host shale are shown in Figure 5. After removal of a low-temperature component, which usually comprises a small fraction of the total NRM (e.g., Figures 5a, 5b, 5c, and 5f), one (e.g., Figures 5a and 5b) or more (e.g., Figures 5c and 5f) magnetization components can be resolved. In geographic coordinates, most components fall into a loosely defined westerly declination cluster with negative and positive shallow to intermediate inclinations (Figure 5g). Other less frequent clusters have northeast-directed declinations with shallow negative inclinations and a southern group with positive intermediate inclinations. A notable feature of the matrix rocks is the absence of steep directions with inclinations exceeding 60° (Figure 5g).

Samples with the distinctive Zebra pattern have highly variable demagnetization behavior even in closely spaced specimens. The variability of vector component diagrams for six sister specimens cut from a single block sample is illustrated in Figure 6. For all samples, a low-temperature component with a direction similar to the present-day field (PDF) direction is removed at 100–200°C. A south-directed component with positive inclination, which is nearly antipodal to the PDF direction, is well resolved in some specimens in the ~200 to ~600°C range (e.g., Figures 6c, 6d, 6e, and 6f). An east-directed component is resolved in the 600–685°C range in only two specimens (Figures 6c and 6d). A high-temperature component (~650–690°C) with steep positive inclination is resolved in four specimens. In specimen ZR_528_b1, the eastward and steep components coexist (Figure 6c), while in specimen ZR_528_b2, where the eastward component is also identified, the steep component is not resolved (Figure 6d). Instead, the highest temperature component seems to be a composite direction between the eastward and southward directions. Overall, four magnetization directions are identified in six sister specimens, with a few intermediate directions that are likely to represent composite components (Figure 6g). A steep positive magnetization component is observed in most samples with the Zebra pattern (Figure 7). This component is typically the highest temperature one in the sample (e.g., Figures 7e–7g), although in a few specimens it unblocks at intermediate temperatures (e.g., Figures 7h and 7i).

Due to the uneven distribution of hematite, Zebra Rock samples should have a pronounced magnetic fabric. Whether such fabric contributes to the remanence direction is impossible to evaluate directly; high coercivities of the Zebra pigment precludes anisotropy of remanent magnetization measurements (e.g., Bilardello & Kodama, 2009) with commercially available equipment. However, we observe the steep remanence in samples with various stripe orientations with respect to the bedding plane—ranging from nearly parallel to

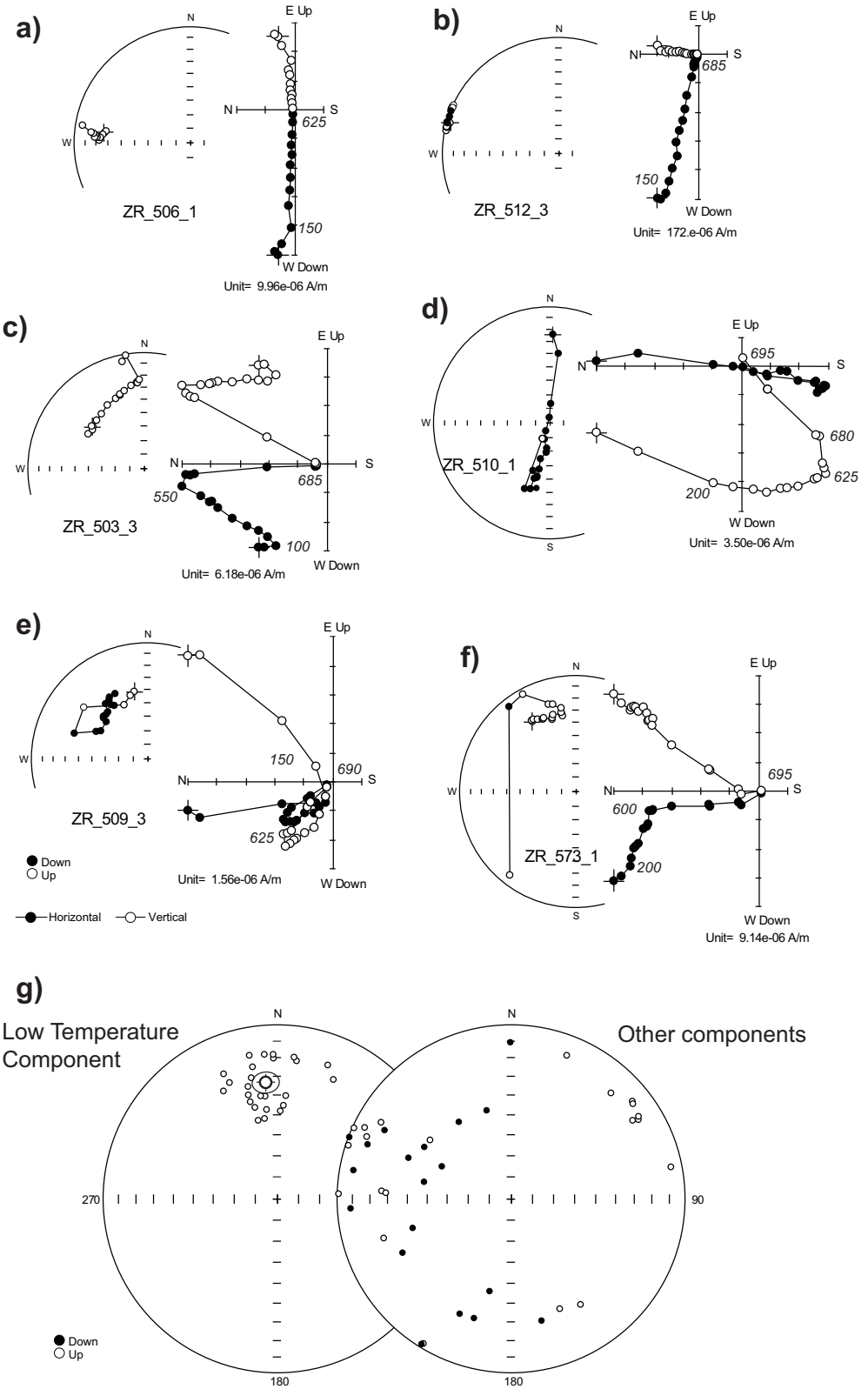

Figure 5. (a–f) Representative vector component diagrams for host shale samples in geographic coordinates. Solid and open symbols represent endpoints projected onto the horizontal and vertical planes, respectively. (g) Stereographic projections with directions isolated from host shale samples. (left) The overprint on all samples due to a present-day field overprint. (right) Other components identified from the studied samples.

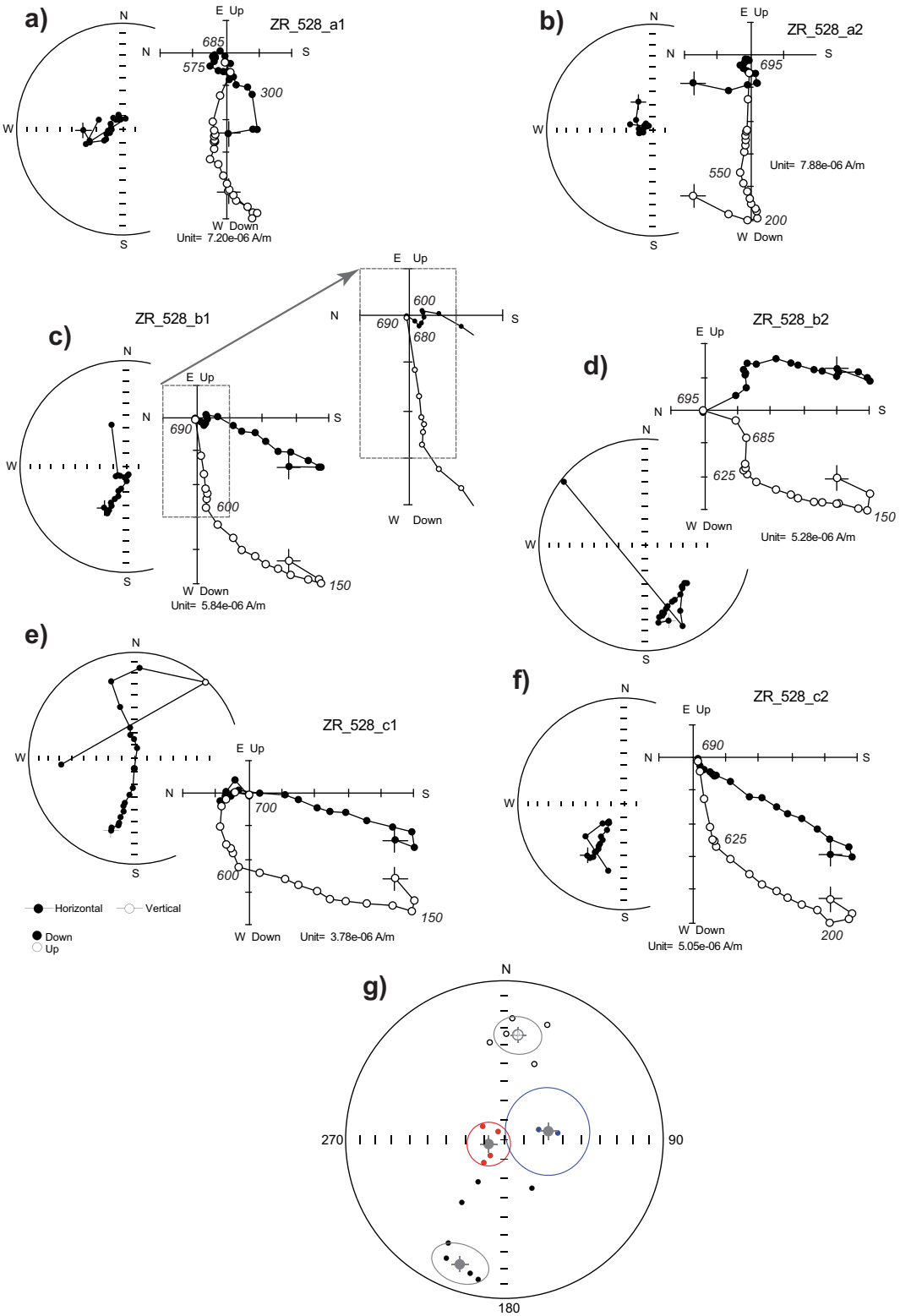

Figure 6. (a–f) Vector component diagrams and stereographic projections for six sister specimens from the block sample ZR_528, in geographic coordinates. (g) Stereographic projection with the four magnetization components (and composite intermediate directions) isolated from the ZR_528 block sample. Each direction represents a single magnetization component identified within one of the six specimens (the directions are color coded for clarity).

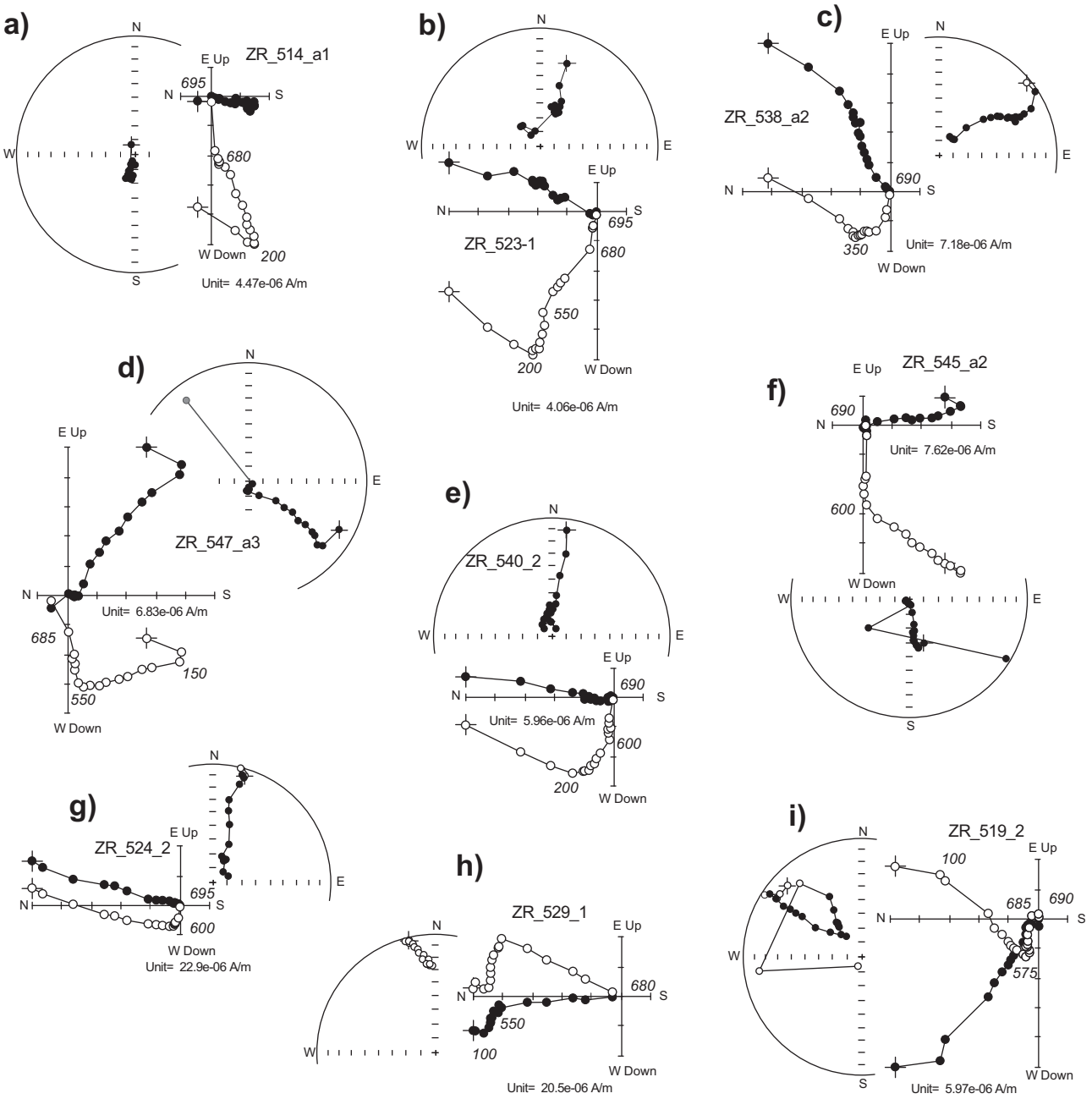

Figure 7. Vector component diagrams for representative samples with the Zebra pattern, in geographic coordinates.

nearly perpendicular to bedding (e.g., Figures 1c–1e). Lack of correlation between the steep remanence and Zebra pattern orientation suggests that the remanence is not affected by magnetic fabric anisotropy.

Individual directions isolated from the studied Zebra Rock samples are shown in Figure 8a in geographic coordinates, and are listed in Table 1. Small bedding attitude variations at the sampling site do not allow a fold test, and no other field tests were available to constrain the age of magnetization components. The components with shallow to intermediate inclinations fall close to the Australian Paleozoic apparent polar wander path (APWP) (Figure 8b and Table 1). However, the steep component that occurs only in samples with distinct Zebra patterning does not resemble any Paleozoic or younger directions. The paleomagnetic pole for the mean "steep" direction is shown in Figure 8b and Table 1, in both geographic and stratigraphic coordinates.

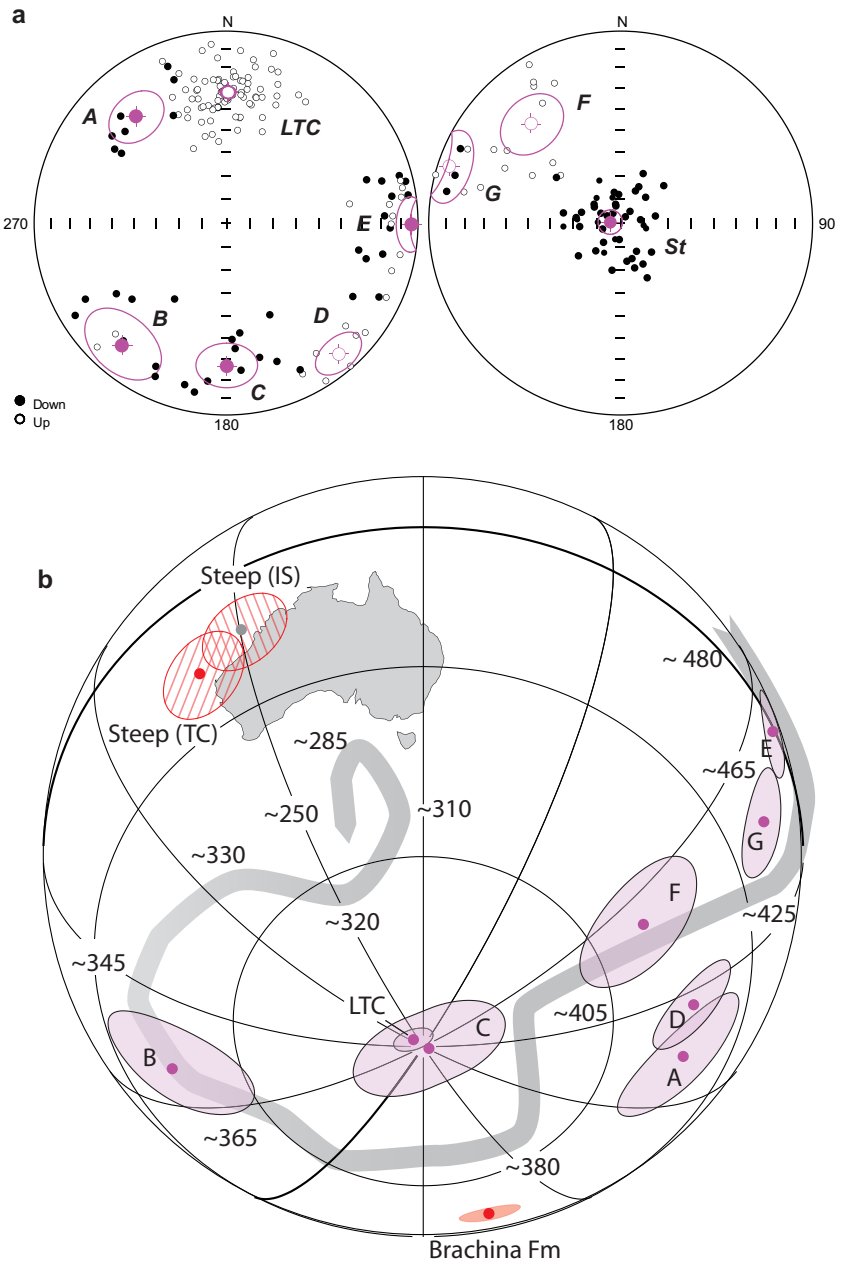

Figure 8. (a) Stereographic projections of magnetization components isolated from samples with the distinct Zebra pattern, in geographic coordinates. LTC = low-temperature component. A-G = seven distinct components identified from stepwise thermal demagnetization data. ST = steep remanence component (as discussed in the text). (b) Paleomagnetic poles calculated from Zebra Rock magnetization components compared to the reference APWP for Australia. Poles are shown in geographic coordinates, except for the characteristic Zebra remanence (steep component) that is shown in both tilt-corrected (TC) and in situ (IS) coordinates. The Paleozoic APWP segment for Australia is after McElhinny et al. (2003). The paleopole from the coeval Brachina Formation (Schmidt & Williams, 2010) is shown for comparison. Poles indicated A-G represent the clusters of paleomagnetic directions shown in Figure 8a.

4. Discussion

4.1. Hematite Formation

Significantly different magnetic properties between the Zebra Rock and host shales likely reflect different hematite pigment formation processes. The red Zebra pigment has a smaller median particle size (lower transition temperature) with wide grain-size distribution (wide transition interval and larger thermal

Table 1
Directions of Characteristic Remanent Magnetization Components From Zebra Rock Samples

		Geographic				Stratigraphic				Paleopole[a]				
Comp	*N*	Dec.	Inc.	*k*	α_{95}	Dec.	Inc.	*k*	α_{95}	Plat.	Plong.	d*p*	d*m*	Paleolatitude
LTC	82	0.9	−32.4	30.6	2.9	2.2	−25.8	23.7	3.3	−88.3	98.9	1.8	3.3	−17.6
A	8	324.4	25.1	21.4	12.2	319.8	28.1	25.8	11.1	44.2	76.8	7.1	13.1	13.2
B	11	225.6	23.7	11.2	14.3	222.6	16.7	12.5	13.5	−45.7	40.4	8.1	15.2	12.4
C	9	179.2	28.8	22.6	11.1	179.8	26.4	22.6	11.1	−88.9	263.6	6.7	12.2	15.4
D	7	139.3	−10.9	47.8	8.8	138.1	−11.6	45.9	9.0	44.3	64.0	4.5	8.9	−5.5
E	23	90.4	3.9	13.5	8.6	90.8	−2.2	13.0	8.7	−0.9	217.3	4.3	8.6	2.0
F	10	319.7	−25.4	18.0	11.7	321.5	−16.5	9.0	16.3	−51.0	217.6	6.8	12.6	−13.3
G	10	289.1	−5.1	24.3	10.0	288.6	−4.5	14.4	13.2	−19.1	222.0	5.0	10	−2.6
Steep	51	296.5	88.2	30.1	3.7	252.5	83.6	30.3	3.7	−14.6	125.7	7.3	7.3	86.4
										−19.6	*116.3*	*7.1*	*7.2*	*77.4*

Note. *N* = number of specimens; Dec. and Inc. = declination and inclination of the site-mean direction (in degrees); α_{95} is the radius of the 95% confidence cone about the mean direction (in degrees); *k* is the Fisher (1953) concentration parameter. Plat., paleopole latitude (in degrees); Plong., paleopole longitude (in degrees); d*p* and d*m* are semiaxes of the 95% cone of confidence about the mean (in degrees).

[a]With the exception of the Steep magnetization component, paleopoles are given in geographic coordinates; no correction for tilt was applied because of subhorizontal bedding at the sampling site. For the Steep component, a paleopole in tilt-corrected coordinates is listed in addition in italics.

hysteresis) and higher degree of structural perfection (lower defect moment). Different bulk coercivities suggest that hematite in Zebra Rock and host shale might have different grain morphology. Particularly high coercivities are typical of pseudocubic hematite (Liu et al., 2010). Somewhat surprisingly for Neoproterozoic rocks, the hematite pigment of Zebra Rock has low thermal stability. Heating leads to significant changes in coercivity and Morin transition parameters. The onset of thermal alteration at 300°C suggests that the Zebra Rock has never been heated to higher temperatures since the time the pattern formed.

The unusual hematite pigment distribution in Zebra Rock suggests that segregation of a precursor phase occurred in a single episode. Ferrihydrite, which has been detected in Zebra Rock by electron paramagnetic resonance in both red and white regions (Boas et al., 2005), was probably the precursor phase. According to Mattievich et al. (2002, 2003), transformation of ferrihydrite to hematite with associated changes in magnetic properties led to formation of a ferronematic liquid crystal in an aqueous medium. Segregation of hematite into red bands is argued to have been driven by interaction of magnetic moments of hematite-coated kaolinite platelets with the geomagnetic field. The results of Jiang et al. (2016) validate this possibility. If this model is correct, it suggests that hematite formed early, during pattern formation. Thus, it possibly preserves a record of the geomagnetic field at the time of rock formation. Mattievich et al. (2003) estimated that hematite particles in the tens of nanometer size range (i.e., superparamagnetic particles) had sufficient magnetic moment to drive segregation in an Earth-like magnetic field. The presence of multiple magnetization components in Zebra Rock without evidence for an additional input of dissolved iron indicates that particle growth through the magnetic blocking volume (or by local recrystallization) continued for a significant amount of time after the segregation episode. Based on comparison of recorded paleomagnetic directions with the Australian Paleozoic APWP (Figure 8b), this amount of time could have been hundreds of millions of years. Recognizable directions, rather than predominantly composite directions (e.g., Figures 6 and 7), also suggest episodic, or localized, rather than continuous grain growth. Subtle ambient temperature and/or confining pressure variations may have served as an on/off switch for grain growth episodes by changing the energy of the system (e.g., Evans et al., 2001). Highly variable demagnetization behavior at small spatial scales, such as the presence of components with similar directions, yet with different relative contributions to the total sample NRM (e.g., Figure 6), is consistent with stochastic chemical grain growth. The main concept of stochastic grain growth theory is that at a given temperature the growth rate of an individual grain is related to its local topology (e.g., Fradkov & Udler, 1994; Pande, 1987; Pande & McFadden, 2010; Thorvaldsen, 1993; Zhao, 1995). Different grain orientations, inhomogeneous impurity distribution, and the effects of neighboring grains result in different growth rates. Overall, extremely slow grain growth and the low thermal stability of Zebra pigment are indicative of low thermodynamic energy. While this is

unusual for Neoproterozoic rocks, the sampled Johnny Cake Shale seems to have avoided significant metamorphic heating.

4.2. Paleomagnetism

Most of the magnetization components isolated from the Zebra Rock and host shales can be identified as Paleozoic overprints by their similarity with the reference Australian APWP (Figure 8b). Although no field tests are available to constrain directly the age of the steep characteristic high-temperature magnetization component, we consider this magnetization as primary for the following reasons. (1) The characteristic remanence direction does not resemble Paleozoic overprint directions (Figure 8b). (2) The steep characteristic magnetization is unique to samples with the Zebra pattern; this component is likely related to the pattern formation episode. (3) The low degree of thermal alteration indicated by our experiments is conducive to preservation of a primary magnetization. (4) The characteristic remanence direction in Zebra Rock is nearly orthogonal to bedding. In the liquid crystal model (Mattievich et al., 2002, 2003), nearly right angles between the bedding plane and the striped pattern in Zebra Rock require a high angle between the geomagnetic field and the preferred clay particle orientation (which in Zebra Rock is parallel to the edge of enclosing strata). Consistency between model prediction and the observed relationship between the paleomagnetic field direction and bedding is a further supporting argument in favor of a primary origin for the "steep" magnetization component.

A paleomagnetic pole calculated for the characteristic Zebra Rock component deviates significantly from Australian Neoproterozoic poles (e.g., Schmidt, 2014). Although currently there is no reliable date for the Zebra Rock, interbasinal chronostratigraphic correlations in Australia from tillite lithostratigraphic correlation and carbon isotopic profiles, with stromatolite and acritarch biostratigraphic correlations, suggest that the Ranford Formation represents an interglacial sequence between the Marinoan and Gaskiers glaciations of the late Neoproterozoic, and, thus, is correlative with the Ediacaran Brachina Formation in South Australia (Corkeron, 2007; Grey & Corkeron, 1998). Discovery of Ediacara-type fossils in the Johnny Cake Shale member of the Ranford Formation (Lan & Chen, 2012) also supports an Ediacaran age for the Formation. The Zebra pole deviates by 67 $\pm$ 9° from the correlative Brachina Pole reported by Schmidt and Williams (2010). Given the nature of the chemical environment that required coincidence of several unusual conditions, formation of the Zebra pattern may not have occurred over a long enough period to have averaged secular variation. It is possible that the Zebra pole, thus, represents a virtual geomagnetic pole (VGP). However, the difference between the Zebra pole and the Brachina Formation pole (presumably the time-averaged paleomagnetic pole) exceeds the deviation expected for normal field behavior, such as secular variation ($\sim$20°) or geomagnetic excursions ($>$45° deviation from the pole; e.g., Butler, 1992). Regardless of whether the Zebra pole is a mean (time-averaged) paleomagnetic pole, or a VGP within the range of normal secular variation, the steep characteristic Zebra remanence likely records an Ediacaran episode when the geomagnetic pole was located near the sampling area. This puts it at odds with paleomagnetic data from the Adelaide Syncline that indicate a shallow magnetization (i.e., a low latitude) for Ediacaran Australia (Schmidt, 2014; Schmidt & Williams, 2010).

Similarly incompatible, shallow and steep, magnetization directions have been observed in Ediacaran rocks at multiple localities in Laurentia, Baltica, and Africa (e.g., Abrajevitch & Van der Voo, 2010). Although the primary versus secondary nature of these components is disputed (e.g., Bono & Tarduno, 2015), the primary nature of several components has been demonstrated by paleomagnetic tests in several cases (e.g., Halls et al., 2015; Robert et al., 2017). The proposed explanations for such incompatible components range from true polar wander (TPW) (e.g., Evans, 1998; Robert et al., 2017), an equatorial dipole (Abrajevitch & Van der Voo, 2010), or an unusually high number of transitional directions (e.g., Halls et al., 2015). So far, no deviating components have been reported from Australia. Schmidt and Williams (2010) and Schmidt (2014) emphasized the lack of discordant directions in the Australian paleomagnetic database to argue against the postulated global TPW event. The steep characteristic remanence in the Zebra Rock pole is likely to be such a discordant direction, and is the first such discordant Ediacaran pole documented from Australia.

A possible reason for why such directions have not been observed previously in Australia is the different mechanism and time scales of magnetization recording processes in Zebra Rock and the sedimentary Brachina Formation. The common recording of dual polarities of discordant directions suggests that an atypical pole position (or a continent in the TPW scenario) across a polarity reversal must have lasted for at least a

few thousand years (Clement, 2004) and probably longer; however, recording of individual VGPs was likely much shorter. Documented incompatible directions are usually recorded as a thermoremanent magnetization (TRM) in rapidly cooled volcanic rocks (e.g., Halls et al., 2015; Meert et al., 2007; Robert et al., 2017). Dendritic magnetite and ilmenite crystals in 590 Ma Grenville dikes, Canada, that host incompatible directions (Halls et al., 2015) suggest cooling rates as high at 0.6–60°C/h (Kretz, 2003). Cooling rates inferred for volcaniclastic deposits range from 1 to 10°C/s for Plinian-fall deposits to 30–0.3°C/yr for the interiors of thick, pyroclastic-flow deposits (Wallace et al., 2003). Thus, cooling through the critical TRM interval 50–100°C below T_C or T_N of the dominant magnetic mineral (magnetite or hematite) would have taken minutes to weeks, and up to a few hundred years for slow cooling volcanic dikes and flows. The steep Zebra Rock component that we interpret to be primary has a single polarity. The duration over which this chemical remanent magnetization component was recorded is likely to be comparable to that of volcanic rocks that recorded similar discordant directions, a few hundred years at most. The likelihood of recording an episode of hundreds of years duration through depositional processes in shallow marine siltstones and fine-grained sandstones of the Brachina Formation (e.g., Preiss, 2000) is low because of the generally slow, unsteady, and discontinuous sedimentation in such environments (e.g., Sadler, 1999).

5. Conclusions

Our study of unusually colored and patterned Zebra Rock, which is found in seams within the Neoproterozoic Johnny Cake Shale member of the Ranford Formation in the Kimberley region, Australia, reveals distinct rock magnetic differences between hematite pigments in Zebra Rock and host shales, which indicate different hematite formation processes in these rock types. The Zebra Rock pigment has higher M_{rs}/M_s, B_c, and B_{cr} values, lower Morin transition temperatures with the transition occurring over a wider temperature interval, larger thermal hysteresis, and lower defect moment. Such differences indicate a smaller median particle size, wider grain-size distribution, and higher degree of structural perfection of hematite in Zebra Rock. Stepwise heating experiments indicate the onset of thermal alteration at 300°C, which suggests that the rocks have not experienced heating to higher temperatures since the Zebra pattern formed.

Stepwise thermal demagnetization of oriented samples reveals short-range, large-scale magnetization variability, with similar component directions, yet with different relative contributions to the total NRM. While magnetization components with shallow to intermediate inclinations isolated from the studied samples can be matched to the Paleozoic Australian APWP, samples with the distinct Zebra pattern also contain a distinct steeply dipping magnetization that was not observed in host shales. Although no field tests could be applied to constrain the age of the steep component, we interpret it to be primary based on its unique association with the Zebra pattern, dissimilarity with younger directions, and evidence for minimal thermal alteration. The steep Zebra Rock remanence likely records an episode when the Ediacaran geomagnetic pole was located near the sampling area. This puts it at odds with previous paleomagnetic data that indicate low Neoproterozoic Australian paleolatitudes. The characteristic Zebra Rock magnetization is the first Australian example of incompatible magnetization directions that have been reported previously from Ediacaran rocks in Laurentia, Baltica, and Africa.

Acknowledgments

We thank Kim Walker and Ruth Duncan from the Zebra Rock Mine, Bruce Livett from the Zebra Rock Gallery, and Dan Read from Top Rockz for interesting discussions and permission to sample Zebra Rock for this study. We acknowledge the Australian Research Council (ARC) through grant FS1001000076 to APR and colleagues that provided a Super Science Fellowship to AA. We thank two anonymous reviewers for constructive review comments. A list of magnetization components isolated from Zebra Rock collection can be found in supporting information Table S1.

References

Abrajevitch, A., Pillans, B. J., & Roberts, A. P. (2014). Haematite pigmentation events and palaeomagnetic recording: Implications from the Pilbara Print Stone, Western Australia. *Geophysical Journal International*, *199*(2), 658–672.

Abrajevitch, A., & Van der Voo, R. (2010). Incompatible Ediacaran paleomagnetic directions suggest an equatorial geomagnetic dipole hypothesis. *Earth and Planetary Science Letters*, *293*(1–2), 164–170.

Bilardello, D., & Kodama, K. P. (2009). Measuring remanence anisotropy of hematite in red beds: Anisotropy of high-field isothermal remanence magnetization (hf-AIR). *Geophysical Journal International*, *178*(3), 1260–1272.

Boas, J. F., Cashion, J. D., Chadwick, J., Clark, M. J., Mackie, R. D., & Mattievich, E. (2005). Electron paramagnetic resonance of defects and Fe^{3+} in Kimberley Zebra Rock. In *16th Natl Congr. Austr. Inst. Phys. Congr. Proc. Handb. Abstr.*, Australia (268 p.).

Bono, R. K., & Tarduno, J. A. (2015). A stable Ediacaran Earth recorded by single silicate crystals of the ca. 565 Ma Sept-Îles intrusion. *Geology*, *43*(2), 131–134.

Butler, R. F. (1992). *Paleomagnetism: Magnetic domains to geologic terranes*. Boston, MA: Blackwell Scientific Publications.

Chadima, M., & Hrouda, F. (2006). Remasoft 3.0 a user-friendly paleomagnetic data browser and analyzer. *Travaux Géophysiques*, *27*, 20–21.

Clement, B. M. (2004). Dependence of the duration of geomagnetic polarity reversals on site latitude. *Nature*, *428*(6983), 637–640.

Corkeron, M. (2007). Cap carbonates' and Neoproterozoic glacigenic successions from the Kimberley region, north-west Australia. *Sedimentology*, *54*, 871–903.

De Boer, C. B., & Dekkers, M. J. (1998). Thermomagnetic behaviour of haematite and goethite as a function of grain size in various non-saturating magnetic fields. *Geophysical Journal International*, *133*(3), 541–552.
Dill, H. G. (2001). The geology of aluminium phosphates and sulphates of the alunite group minerals: A review. *Earth-Science Reviews*, *53*, 35–93.
Dow, D. B., & Gemuts, I. (1969). *Geology of the Kimberley Region, Western Australia: The East Kimberley* (Vol. 120). Perth, Australia: Geological Survey of Western Australia.
Dunlop, D. J., & Özdemir, Ö. (1997). *Rock magnetism: Fundamentals and frontiers*. Cambridge, UK: Cambridge University Press.
Evans, B., Renner, J., & Hirth, G. (2001). A few remarks on the kinetics of static grain growth in rocks. *International Journal of Earth Sciences*, *90*(1), 88–103.
Evans, D. A. (1998). True polar wander, a supercontinental legacy. *Earth and Planetary Science Letters*, *157*, 1–8.
Fisher, R. A. (1953). Dispersion on a sphere. *Proceedings of the Royal Society of London A*, *217*, 295–305.
Fradkov, V. E., & Udler, D. (1994). Two-dimensional normal grain growth: Topological aspects. *Advances in Physics*, *43*(6), 739–789.
Geidans, L. (1981). Zebra rock of Western Australia. *Geological Society of Australia, Abstracts*, *3*, 22.
Grey, K., & Corkeron, M. (1998). Late Neoproterozoic stromatolites in glacigenic successions of the Kimberley region, Western Australia: Evidence for a younger Marinoan glaciation. *Precambrian Research*, *92*(1), 65–87.
Halls, H. C., Lovette, A., Hamilton, M., & Söderlund, U. (2015). A paleomagnetic and U–Pb geochronology study of the western end of the Grenville dyke swarm: Rapid changes in paleomagnetic field direction at ca. 585 Ma related to polarity reversals? *Precambrian Research*, *257*, 137–166.
Hancock, P. M. (1968). Location and investigation of zebra rock occurrences, East Kimberley region (West. Austr. Geol. Surv. Ann. Rep. 1968, pp. 27–28). Perth, Australia: Geological Survey of Western Australia.
Hobson, R. A. (1930). Zebra rock from Kimberley. *Journal of the Royal Society of Western Australia*, *16*, 57–70.
Jamtveit, B., & Hammer, Ø. (2012). Sculpting of rocks by reactive fluids. *Geochemical Perspectives Letters*, *1*(3), 341–342.
Jiang, Z. X., Liu, Q. S., Dekkers, M. J., Barrón, V., Torrent, J., & Roberts, A. P. (2016). Control of Earth-like magnetic fields on the transformation of ferrihydrite to hematite and goethite. *Scientific Reports*, *6*, 30395. https://doi.org/10.1038/srep30395
Kirschvink, J. L. (1980). The least-squares line and plane and the analysis of palaeomagnetic data. *Geophysical Journal of the Royal Astronomical Society*, *62*, 699–718.
Kretz, R. (2003). Dendritic magnetite and ilmenite in 590 Ma Grenville dikes near Otter Lake, Quebec, Canada. *Canadian Mineralogist*, *41*, 1049–1059.
Lan, Z. W., & Chen, Z. Q. (2012). Possible animal body fossils from the late Neoproterozoic interglacial successions in the Kimberley region, northwestern Australia. *Gondwana Research*, *21*(1), 293–301.
Larcombe, C. O. G. (1924). *Rock specimens from Ord River and Oakover River, respectively* (Geol. Surv. West. Austr., Ann. Rep. 19). Perth, Australia: Geological Survey of Western Australia.
Larcombe, C. O. G. (1926). *Some rocks from four miles east of Argyle Station, Ord River, King district, Kimberley division* (Geol. Surv. West. Austr., Ann. Rep., 23). Perth, Australia: Geological Survey of Western Australia.
Liu, C., Ge, K., Zhang, C., Liu, Q., Deng, C., & Zhu, R. (2011). Nature of remagnetization of Lower Triassic red beds in southwestern China. *Geophysical Journal International*, *187*(3), 1237–1249.
Liu, Q., Barrón, V., Torrent, J., Qin, H., & Yu, Y. (2010). The magnetism of micro-sized hematite explained. *Physics of the Earth and Planetary Interiors*, *183*(3–4), 387–397.
Loughnan, F. C., & Roberts, F. I. (1990). Composition and origin of the 'zebra rock' from the East Kimberley region of Western Australia. *Australian Journal of Earth Sciences*, *37*(2), 201–205.
Mattievich, E., Chadwick, J., Cashion, J. D., Boas, J. F., Clark, M. J., & Mackie, R. D. (2002). A ferronematic liquid crystal phase in Precambrian zebra rock from the Kimberley region. In *26th Ann. Cond. Matt. Phys. Meet. Conf. Handb*., Australia (146 p.).
Mattievich, E., Chadwick, J., Cashion, J. D., Boas, J. F., Clark, M. J., & Mackie, R. D. (2003). Macroscopic ferronematic liquid crystals determine the structure of Kimberley Zebra Rock. In *27th Ann. Cond. Matt. Phys. Meet. Conf. Handb*., Australia (91 p.).
McElhinny, M. W., Powell, C. M., & Pisarevsky, S. A. (2003). Paleozoic terranes of eastern Australia and the drift history of Gondwana. *Tectonophysics*, *362*(1–4), 41–65.
Meert, J. G., Walderhaug, H. J., Torsvik, T. H., & Hendriks, B. W. (2007). Age and paleomagnetic signature of the Alnø carbonatite complex (NE Sweden): Additional controversy for the Neoproterozoic paleoposition of Baltica. *Precambrian Research*, *154*(3–4), 159–174.
Morin, F. J. (1950). Magnetic susceptibility of alpha-Fe_2O_3 and alpha-Fe_2O_3 with added titanium. *Physical Review*, *78*, 819–820.
Özdemir, Ö., & Dunlop, D. J. (2006). Magnetic memory and coupling between spin-canted and defect magnetism in hematite. *Journal of Geophysical Research*, *111*, B12S03. https://doi.org/10.1029/2006JB004555
Özdemir, Ö., Dunlop, D. J., & Berquo, T. S. (2008). Morin transition in hematite: Size dependence and thermal hysteresis. *Geochemistry, Geophysics, Geosystems*, *9*, Q10Z01. https://doi.org/10.1029/2008GC002110
Pande, C. S. (1987). On a stochastic theory of grain growth. *Acta Metallurgica*, *35*, 2671–2678.
Pande, C. S., & McFadden, G. B. (2010). Self-similar grain size distribution in three dimensions: A stochastic treatment. *Acta Materialia*, *58*(3), 1037–1044.
Park, J. K. (1997). Paleomagnetic evidence for low-latitude glaciation during deposition of the Neoproterozoic Rapitan Group, Mackenzie Mountains, NWT, Canada. *Canadian Journal of Earth Sciences*, *34*, 34–49.
Preiss, W. V. (2000). The Adelaide Geosyncline of South Australia and its significance in Neoproterozoic continental reconstruction. *Precambrian Research*, *100*, 21–63.
Ricordel, C., Parcerisa, D., Thiry, M., Moreau, M. G., & Gómez-Gras, D. (2007). Triassic magnetic overprints related to albitization in granites from the Morvan massif (France). *Palaeogeography Palaeoclimatology Palaeoecology*, *251*(2), 268–282.
Robert, B., Besse, J., Blein, O., Greff-Lefftz, M., Baudin, T., Lopes, F., et al. (2017). Constraints on the Ediacaran inertial interchange true polar wander hypothesis: A new paleomagnetic study in Morocco (West African Craton). *Precambrian Research*, *295*, 90–116.
Roberts, A. P., Cui, Y., & Verosub, K. L. (1995). Wasp-waisted hysteresis loops: Mineral magnetic characteristics and discrimination of components in mixed magnetic systems. *Journal of Geophysical Research*, *100*(B9), 17909–17924.
Ross, C. S., & Kerr, P. F. (1930). The kaolin minerals. *Journal of the American Ceramic Society*, *13*(3), 151–160.
Sadler, P. M. (1999). The influence of hiatuses on sediment accumulation rates. *GeoResearch Forum*, *5*(1), 15–40.
Schmidt, P. W. (2014). A review of Precambrian palaeomagnetism of Australia: Palaeogeography, supercontinents, glaciations and true polar wander. *Gondwana Research*, *25*(3), 1164–1185.
Schmidt, P. W., & Williams, G. E. (2010). Ediacaran palaeomagnetism and apparent polar wander path for Australia: No large true polar wander. *Geophysical Journal International*, *182*(2), 711–726.
Schroeer, D., & Nininger, R. C. (1967). Morin transition in α-Fe_2O_3 microcrystals. *Physical Review Letters*, *19*(11), 632–634.

Tauxe, L., Mullender, T. A. T., & Pick, T. (1996). Potbellies, wasp-waists, and superparamagnetism in magnetic hysteresis. *Journal of Geophysical Research*, *101*(B1), 571–583.

Thorne, A. M., Sheppard, S., & Tyler, I. M. (1999). Lissadell, Western Australia. In *1:250 000 Geological map series and explanatory notes*, *SE 52-2* (2nd ed., 68 p.). Geological Survey of Western Australia.

Thorvaldsen, A. (1993). Grain growth as a stochastic process. *Acta Metallurgica et Materialia*, *41*, 1347–1357.

Wallace, P. J., Dufek, J., Anderson, A. T., & Zhang, Y. (2003). Cooling rates of Plinian-fall and pyroclastic-flow deposits in the Bishop Tuff: Inferences from water speciation in quartz-hosted glass inclusions. *Bulletin of Volcanology*, *65*, 105–123.

Zhao, X. (1995). About the stochastic behaviour in grain growth. *Scripta Metallurgica et Materialia*, *33*, 1081–1086.

Zijderveld, J. D. A. (1967). A.C. demagnetization of rocks. In D. W. Collinson, K. M. Creer, & S. K. Runcorn (Eds.), *Methods in palaeomagnetism* (pp. 256–286). Amsterdam, the Netherlands: Elsevier.